PNAS RESEARCH ARTICLE | MEDICAL SCIENCES OPEN ACCESS

Brain aerobic glycolysis and resilience in Alzheimer disease

Manu S. Goyal[a,b,c,d,e,1], Tyler Blazey[a,c], Nicholas V. Metcalf[a,c], Mark P. McAvoy[a,c,f], Jeremy F. Strain[b,c], Maryam Rahmani[a,c], Tony J. Durbin[a,c], Chengjie Xiong[d], Tammie L.-S. Benzinger[a,c,d], John C. Morris[b,d], Marcus E. Raichle[a,b,c,d,e,g,h,1], and Andrei G. Vlassenko[a,c,d]

Contributed by Marcus E. Raichle; received July 18, 2022; accepted January 4, 2023; reviewed by Robert C. Cumming and Klaus-Armin Nave

The distribution of brain aerobic glycolysis (AG) in normal young adults correlates spatially with amyloid-beta (Aβ) deposition in individuals with symptomatic and preclinical Alzheimer disease (AD). Brain AG decreases with age, but the functional significance of this decrease with regard to the development of AD symptomatology is poorly understood. Using PET measurements of regional blood flow, oxygen consumption, and glucose utilization—from which we derive AG—we find that cognitive impairment is strongly associated with loss of the typical youthful pattern of AG. In contrast, amyloid positivity without cognitive impairment was associated with preservation of youthful brain AG, which was even higher than that seen in cognitively unimpaired, amyloid negative adults. Similar findings were not seen for blood flow nor oxygen consumption. Finally, in cognitively unimpaired adults, white matter hyperintensity burden was found to be specifically associated with decreased youthful brain AG. Our results suggest that AG may have a role in the resilience and/or response to early stages of amyloid pathology and that age-related white matter disease may impair this process.

Alzheimer's disease | aerobic glycolysis | resilience | aging | white matter hyperintensities

Significance

Brain aerobic glycolysis (AG) decreases with age and correlates regionally with amyloid-beta deposition in Alzheimer disease (AD). Using PET measurements of AG, this study now demonstrates that brain AG loses its youthful pattern in cognitively impaired individuals. In cognitively unimpaired individuals, however, the youthful pattern of brain AG is preserved/heightened in the presence of amyloid deposition, yet conversely decreased in the presence of aging-related white matter hyperintensities. These findings suggest that brain AG changes dynamically according to aging-related pathology, with implications for the development and progression of AD.

The healthy human brain largely relies upon glucose to fuel mitochondrial respiration. Yet, in young adults, a portion of resting glucose consumption exceeds that predicted by oxygen consumption rates (1). Though the role(s) of this excess glucose utilization, i.e., aerobic glycolysis (AG), remain uncertain, some studies suggest that AG in the brain may support neurite outgrowth (2, 3), myelination (4–7), learning (8, 9), reducing oxidative stress (10), rapid and anticipatory neuronal activity (11), and microglial activity (12, 13). AG in the young adult occurs more so in regions that are transcriptionally neotenous and evolutionarily expanded in humans (14). Prior studies in humans demonstrate that brain AG decreases on average in healthy older adults, based on whole brain quantitative measurements (15, 16) as well as in terms of its regional pattern in young adults (17). Moreover, sex influences the youthful pattern of brain glycolysis, being relatively more preserved in cognitively unimpaired aging females than in males (18).

AG in the human brain is also affected by Alzheimer disease (AD). Whole brain estimates show that early AD is associated with a significant decrease in glucose consumption rates compared to a relatively smaller change in oxygen consumption (19–21). Interestingly, amyloid deposition in both cognitively intact and impaired adults follows a regional pattern that matches that of brain AG in young adults (22, 23). Although several studies have studied total regional brain glucose consumption in relation to cognitive impairment with ^{18}FDG-PET alone, none to our knowledge has studied how regional AG is specifically affected, as compared to the larger component of brain glucose use that occurs for oxidative phosphorylation.

Here we investigate regional brain AG in AD by combining ^{18}FDG-PET with ^{15}O-labeled water (H_2O), oxygen (O_2), and carbon monoxide (CO) positron emission tomography (PET) to estimate glucose and oxygen metabolism together—and thereby AG—in individuals further characterized with amyloid imaging and cognitive testing. Our primary hypotheses were that youthful brain AG will be reduced in cognitively impaired individuals and preserved in cognitively intact individuals with biomarker-defined (i.e., brain amyloid positive) AD, as a reflection of brain resilience to AD pathology.

Results

Study Overview. All research participants provided informed consent, and all study procedures were approved by the Washington University School of Medicine Institutional Review Board. A total of 353 multi-tracer metabolic PET sessions were performed in 285 adult individuals (25 to 92 y old, 55% female) between the years of 2013 and 2021. Portions of these data, now labeled as the Aging Metabolism & Brain Resilience ("AMBR") study, have been published previously (17, 18, 23–25). Age, sex, amyloid positivity, and cognitive status were defined for each individual and each of their PET imaging session(s).

Author contributions: M.S.G., J.C.M., M.E.R., and A.G.V. designed research; M.S.G., J.S., M.R., T.J.D., T.B., and A.G.V. performed research; M.S.G., T.B., N.V.M., M.P.M., M.R., C.X., T.L.-S.B., J.C.M., and A.G.V. analyzed data; and M.S.G., M.E.R., and A.G.V. wrote the paper.

Reviewers: R.C.C., Western University; and K.-A.N., Max Planck Institute for Multidisciplinary Sciences.

Competing interest statement: The authors have organizational affiliations to disclose, J.C.M. obtains consulting fees from the Barcelona Brain Research Center and is on the T.S. Srinivasan Advisory Board in Chennai, India.

Copyright © 2023 the Author(s). Published by PNAS. This open access article is distributed under Creative Commons Attribution-NonCommercial-NoDerivatives License 4.0 (CC BY-NC-ND).

[1]To whom correspondence may be addressed. Email: goyalm@wustl.edu or mraichle@wustl.edu.

Published February 6, 2023.

Amyloid status was unavailable in 80 sessions, including in only 18 individuals ≥60 y old and in 62 individuals <60 y old; note that all 40 participants <60 y old who underwent amyloid PET imaging were found to be negative. Accordingly, absent amyloid status was considered to be amyloid negative for statistical analyses unless proven otherwise. Cognitive status was typically defined using the Clinical Dementia Rating® (CDR®) scale, specifically using the sum-of-boxes score; when CDR could not be fully completed (n = 39), cognitive status (normal versus impaired) was instead inferred from additional cognitive testing data. Further details on study procedures are provided below (*Methods*).

From the metabolic PET measures, the glycolytic index (GI, a relative measure of AG), cerebral metabolic rate of glucose (CMRGlc), cerebral metabolic rate of oxygen ($CMRO_2$), and cerebral blood flow (CBF) were calculated and partial volume corrected to regions defined by the Desikan–Killiany atlas and FreeSurfer subcortical parcellations. Symptomatic and "preclinical" (i.e., asymptomatic) AD were defined as individuals with brain amyloid positivity and with cognitive impairment versus without cognitive impairment, respectively.

Analysis Overview. For each PET session and independent metabolic measure (GI, CMRGlc, $CMRO_2$, and CBF), a "youthful pattern" was defined based on its correlation to average gray matter regional values calculated in a separate, previously published but re-processed dataset comprising a cohort of young healthy adults ("N33 cohort," 20 to 34 y old) (Fig. 1) (26). The N33 cohort was used to define the youthful pattern for each metabolic parameter in order to avoid biasing results derived from the larger AMBR cohort. However, as the N33 data were acquired approximately a decade prior with different scanner technology, an outlier region (the pars orbitalis) was identified and was removed from further analysis a priori. The AMBR data were subjected to quantile normalization for each metabolic measure to remove "batch" effects that could have arisen during the 9 y of data collection. A Spearman rank correlation *rho* was then calculated for each PET session in the AMBR study as compared to the group results from the N33 cohort to calculate the "youthful metabolic index" of each metabolic measurement at the time of that PET session. These measures were subsequently related to age, sex, amyloid positivity, and cognitive status using generalized linear and mixed models, as computed in R with missing observations omitted.

Youthful Brain Metabolism Decreases Variably with Age and Sex. For all metabolic measures, the youthful pattern was maintained in young adults from the AMBR cohort (Fig. 2). With increasing age, this youthful pattern for all metabolic parameters was variably maintained, with increasing degrees of inter-individual variability in patterns of brain metabolism, particularly for GI.

Prior observations on a subset of these data (obtained prior to 2017) suggested that the youthful pattern of brain metabolism is more typically preserved in cognitively intact females than in males (18). Subsequent studies using brain age estimations have reported similar findings with ^{18}FDG-PET and brain MRI (27–29). Here, female sex was again associated with a higher youthful GI index when controlling for age and amyloid status ($P < 0.05$). This was true also for the youthful $CMRO_2$ index ($P < 0.005$), but not significantly so for the youthful CMRGlc and CBF indices. With a smaller subset of the data obtained since 2017 in cognitively unimpaired individuals (n = 163), age but not sex remained significant, and further analysis found a sex-by-age interaction to be significant ($P < 0.05$) such that the youthful GI index declined faster for males than females with increasing age. Given these findings, age and sex were included as covariates in the subsequent analyses.

Cognitive Impairment Is Associated with Decreased Youthful Brain Glycolysis. Cognitive impairment, as measured by CDR sum of boxes, was associated with age ($P < 0.005$), male sex ($P < 0.05$), and amyloid positivity ($P < 0.001$). Cognitive impairment was further highly associated with decreased youthful GI index ($P < 0.001$) and youthful CMRGlc index ($P < 0.05$), controlling for age, sex, and amyloid status. Moreover, loss of youthful GI was associated with AD specifically ($P < 0.05$), controlling for age and sex, as well as with cognitive impairment across amyloid positive individuals ($P < 0.01$). However, neither the youthful $CMRO_2$ nor CBF indices were significantly associated with cognitive impairment. These results suggest that early cognitive impairment is associated with changes specifically in glycolysis.

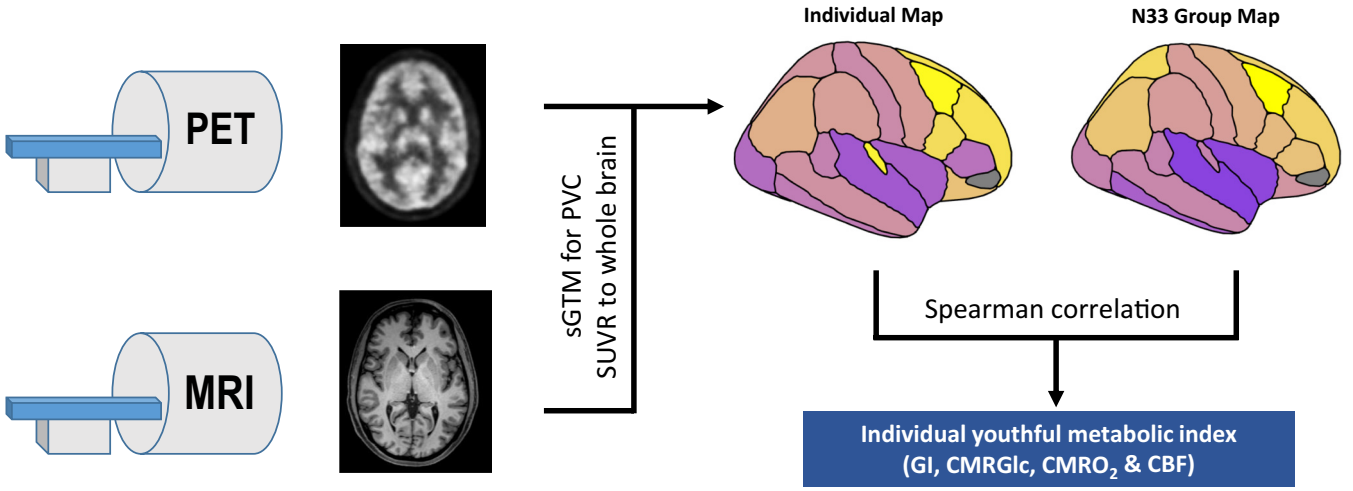

Fig. 1. Schematic overview of youthful brain metabolism calculation. Separate resting PET and MRI scans were obtained in individuals. PET scans were preprocessed and then combined with MRI to calculate partial volume corrected regional standardized uptake value ratio (SUVR) values in the gray matter. Each individual map of brain metabolism and CBF was then compared to the corresponding group map obtained in the separate N33 young adult cohort using a Spearman correlation. The final *rho* value was used as the "youthful metabolic index" for that individual and specific metabolic parameter (GI, FDG, oxygen metabolism, and CBF). (Figures are intended for schematic purposes only.)

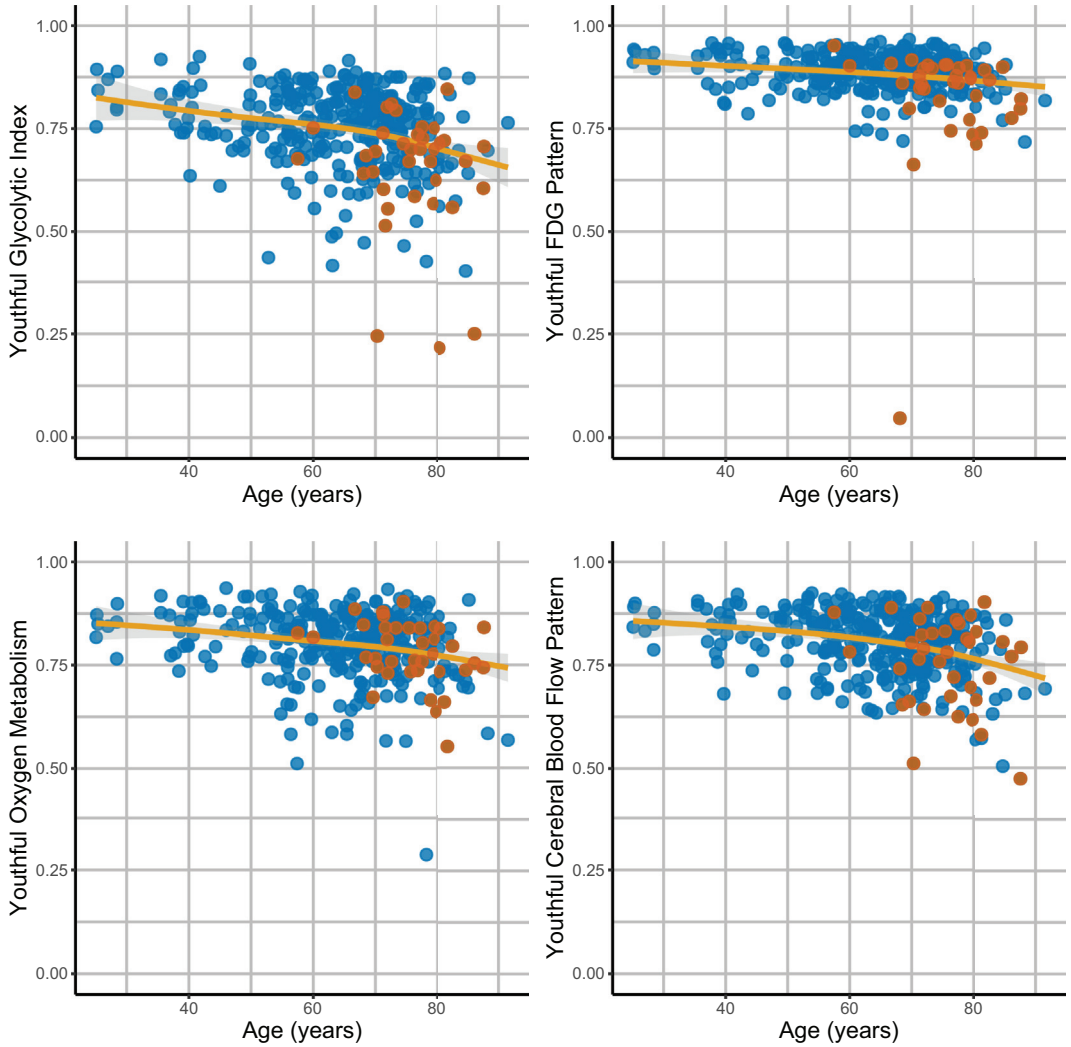

Fig. 2. Differences in the youthful pattern of brain metabolism with age and cognitive impairment. A youthful metabolic index was calculated for AG (GI), CMRGlc (FDG), oxygen metabolism ($CMRO_2$), and CBF (Fig. 1). This was calculated for each of the 353 PET sessions. All indices on average decreased with age (solid lines are generalized additive model (gam) fits with shaded bars reflecting 95% CI). However, this occurred variably across individuals, with some individuals showing a preserved youthful pattern, whereas others showing a decrease in the index. Cognitively impaired individuals (red dots) were more likely to have decreased youthful GI and CMRGlc indices. This was not true, however, for $CMRO_2$ nor CBF.

Cognitive Resilience Is Associated with Preserved Youthful Brain Glycolysis. If loss of the youthful glycolysis pattern during early cognitive impairment is due to direct effects of amyloid deposition rather than downstream neurodegeneration, we would predict that the youthful GI index would be lower also in amyloid positive, cognitively intact individuals. However, when restricting our analysis to individuals with CDR = 0, we did not find this relationship. Instead, amyloid positivity in cognitively intact individuals correlated with higher youthful GI index ($P < 0.01$), suggesting that preservation of AG in the typical glycolytic areas of youth is associated with asymptomatic presence of brain amyloid (Fig. 3).

Given the presence of longitudinally repeated measures in a subset of individuals within the AMBR dataset, a mixed effects model was constructed to account for subjects as a random effect. The youthful GI index was further normalized using a Yeo–Johnson transformation (30). This model again confirmed that the youthful GI index was, on average, higher in amyloid positive, cognitively intact individuals ($P < 0.05$). The same analysis for total CMRGlc, $CMRO_2$, and CBF did not reveal a similar significant relationship for any of these other metabolic parameters. Thus, the association between youthful brain metabolism and cognitive resilience in amyloid positive individuals is specific to brain AG.

Specific Brain Regions Show Reduced AG in Aging and AD. The results above investigate the preservation or loss of a youthful regional pattern of metabolism. This analysis was prescribed a priori to maximize signal-to-noise by using an omnibus measure of regional brain metabolism. However, effects of AD on brain metabolism may extend beyond a decrease in the youthful pattern of brain metabolism. We therefore computed region-by-region generalized regression models to explore the effects of age and AD on group-normalized GI within each region independently. As our metabolic data are not quantitative, only regions with significant negative changes in metabolism are included here, accounting for prior studies that demonstrate that whole brain glycolysis quantitatively decreases with age and in Alzheimer's disease (14–15, 16–21).

Increased age was associated with decreases in GI in the superior frontal, superior parietal, caudal middle frontal, medial orbitofrontal, and entorhinal cortices (Fig. 4). These age-related changes mirror those regions with the highest GI in young healthy adults (see Fig. 1, N33 group average). Controlling for

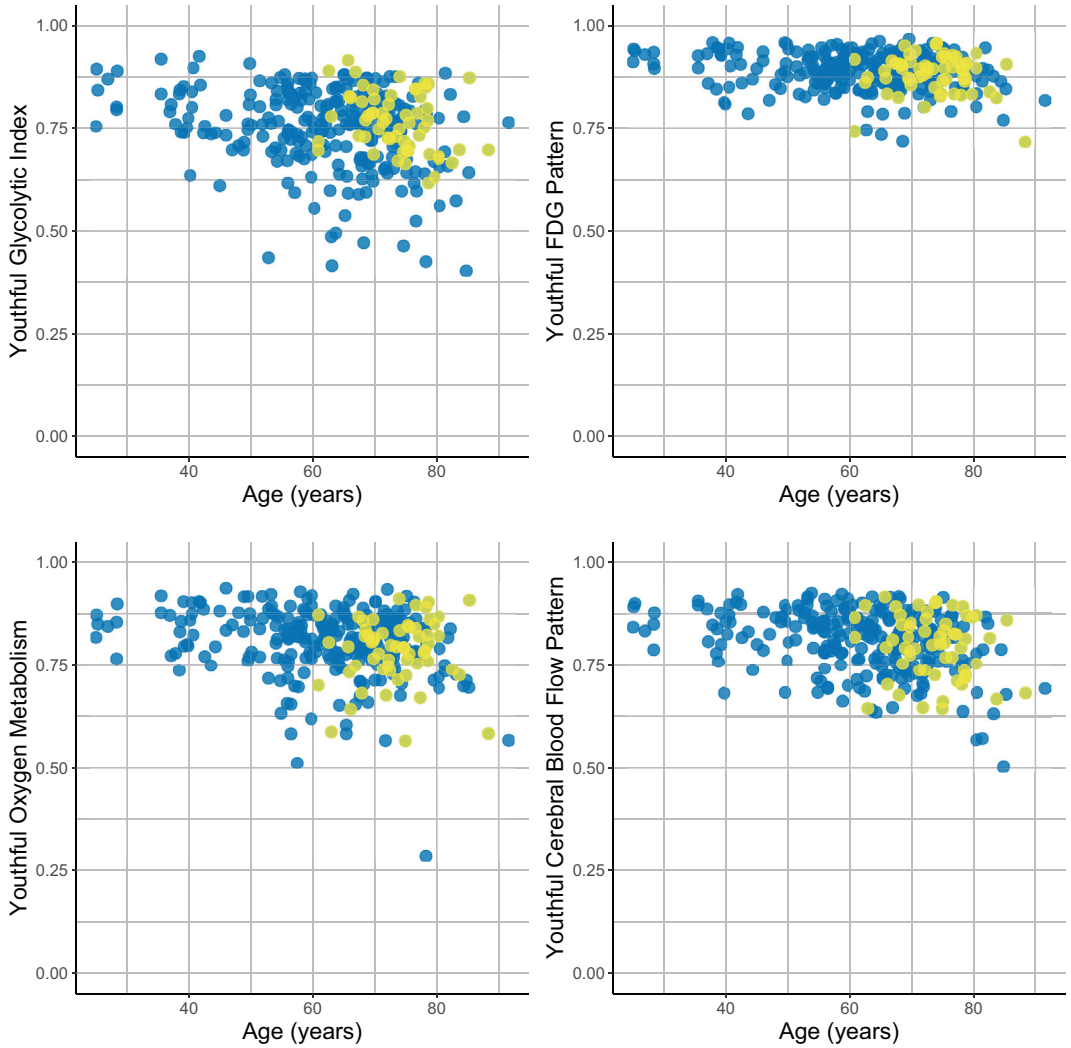

Fig. 3. Association of amyloid positivity with youthful brain metabolism. Correlations to the youthful pattern of GI, FDG, oxygen metabolism, and CBF were measured for each individual PET session (Fig. 1). In this analysis, only the 313 sessions in cognitively unimpaired individuals were included. Among these individuals, known amyloid positivity (yellow dots) was associated with relatively preserved youthful GI as compared to other adults, adjusting for age and sex. This was not true for CMRGlc, $CMRO_2$ nor CBF. Blue dots reflect amyloid negativity or unknown status (presumed negative).

age and sex, AD status was associated with significantly reduced GI in the rostral middle frontal, inferior temporal, inferior parietal, lateral orbitofrontal, middle temporal cortices, and precuneus (Fig. 4).

White Matter Hyperintensity Burden Is Specifically Associated with Reduced AG. White matter hyperintensities (WMH) are nearly ubiquitous in the aged human brain, though the volume of WMH varies considerably across individuals; higher volumes are associated with increased risk of cognitive decline. Given that WMH are located along tracts connecting gray matter regions, increased WMH burden might be a key factor that reduces gray matter AG in the aging brain. A recent study from our lab on a small selected subset of these data used a different analytical approach to focus on how WMH burden influences white matter metabolism; this study found relatively reduced total gray matter glycolysis in older adults with significant WMH (25). To reproduce this preliminary finding with an independent sample, now controlled for amyloid status, we applied the approach developed here in the present study to determine whether WMH volumes might also correlate with reduction in the youthful GI index.

We acquired 1 mm^3 isotropic fluid attenuated inversion recovery (FLAIR) sequences during 104 PET sessions in cognitively unimpaired individuals of the AMBR cohort. WMH were then segmented using intensity thresholding, manual selection of lesions, re-thresholding, and quality control (see *Methods* below for details). Since WMH volumes fit a log-normal distribution in this cohort, they were then log transformed before comparing to brain AG and the other metabolic measures. Controlling for age, sex, and amyloid status, global WMH volumes were significantly associated with reduced youthful GI index ($P < 0.002$) (Fig. 5*A*). This was not true for the other metabolic measures ($P > 0.05$; Fig. 5*B*).

Discussion

Aging is associated with increased inter-individual variability in a variety of domains, including those related to brain function, structure, and neurodegeneration (31–33). Here, we show that aging is similarly associated with increasingly variable changes in brain

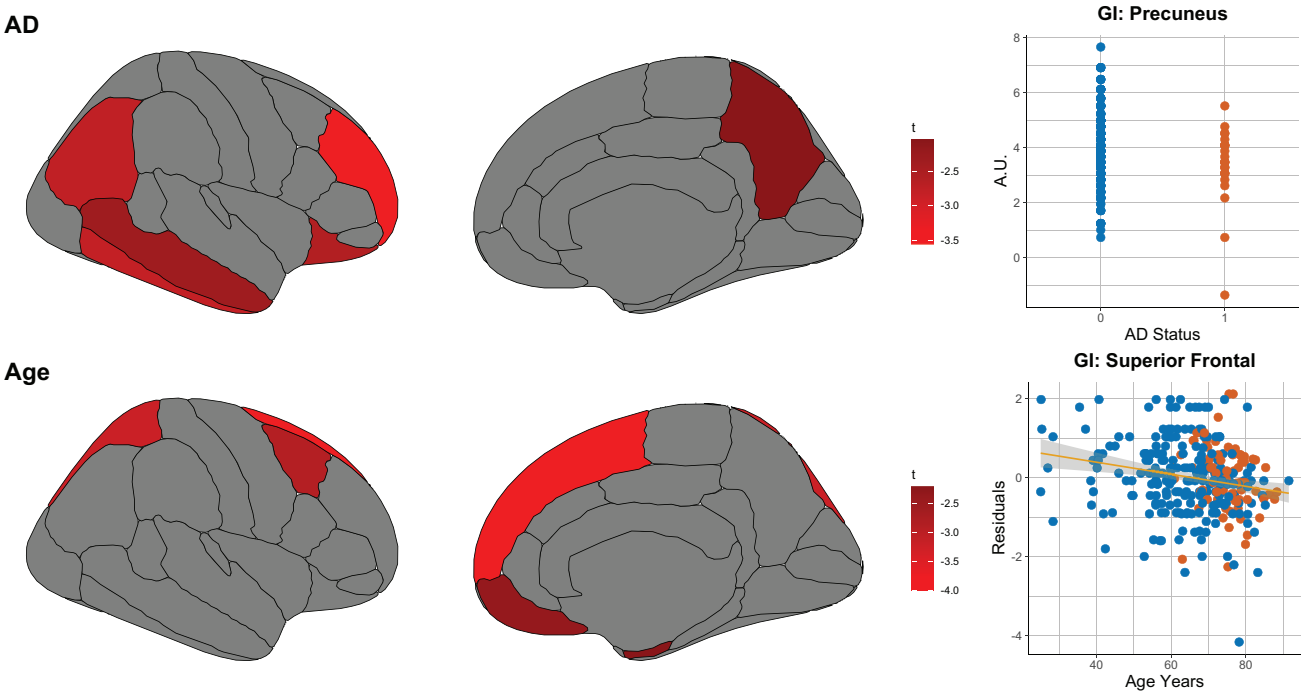

Fig. 4. Associations of regional glycolysis (GI) with aging and AD. The associations of aging and symptomatic AD with GI were explored at a regional level. Regression models were constructed for each independent gray matter region relating GI to age, sex, and AD and subject as a random effect. As this was an exploratory non-quantitative analysis, only regions showing a significant decrease (defined as t-score < −1.96, uncorrected) in GI are shown here, noting that both age and AD are known to be associated with lower whole brain AG (17, 19, 20). AD was associated with decreases in the precuneus, prefrontal, lateral parietal, and temporal regions. Aging was associated with relative decreases primarily in medial frontal and dorsal frontal and parietal areas, consistent with that reported previously. (In the upper right graph, blue and red dots reflect individuals without and with symptomatic Alzheimer disease, respectively. In the lower right graph, blue and red dots reflect individuals without and with brain amyloid positivity, respectively.)

metabolism. As previously reported in a subset of these data, sex accounts for some of this inter-individual variability. Now, we find that early cognitive impairment is associated with loss of the youthful pattern of brain AG and total glucose use, but not in the pattern of $CMRO_2$ nor CBF. This parallels our prior PET study showing that loss of brain AG is specifically associated with tau deposition in AD (24), as well as other whole brain studies of brain metabolism using the invasive Kety-Schmidt technique, where brain glucose consumption rates were shown to fall first during early stages of dementia, followed by decreases in oxygen consumption in later stages of dementia (19–21). The reasons for a selective association between early symptomatic AD and loss of brain glycolysis are not yet clear, but this finding argues against ischemic processes and primary mitochondrial failure as causing a transition to early AD, since both of these would be expected to initially reduce $CMRO_2$ and CBF similar to or more so than glycolysis.

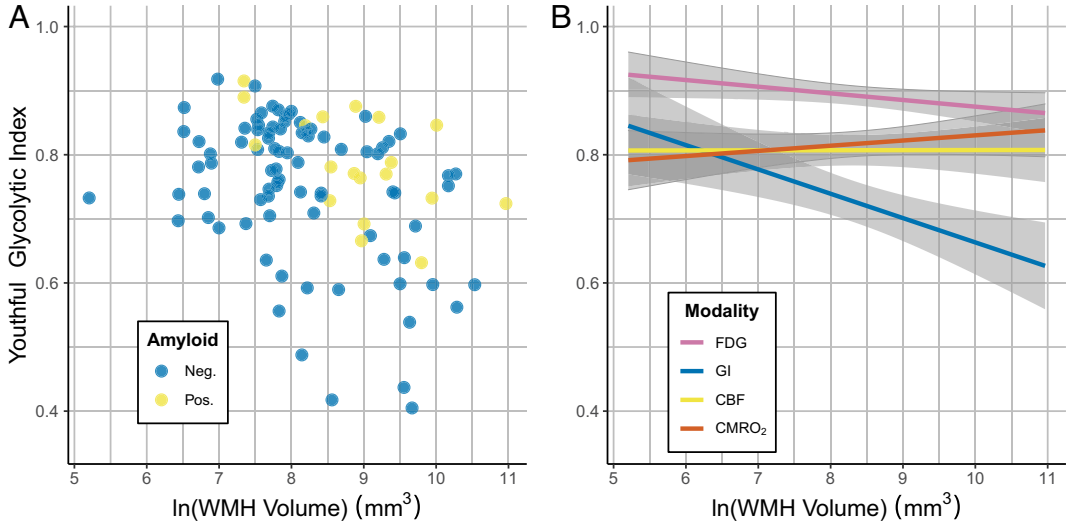

Fig. 5. Association of WMH with youthful brain metabolism in cognitively normal individuals. (*A*) WMH volume (log transformed) was negatively associated with the youthful pattern of AG (GI) ($P < 0.002$). Amyloid positive participants are shown in yellow and negative individuals in blue. (*B*) Model predictions for the association between youthful metabolic indices and WMH volume are shown for males (similar findings are seen in females). Unlike brain AG ("GI," blue), neither total glucose consumption ("FDG," pink), blood flow ("CBF," yellow), nor oxygen consumption ("$CMRO_2$," red) was significantly associated with WMH volume ($P > 0.05$). 95% CIs are shown in gray. All models in (*A*) and (*B*) are adjusted for age, sex, and amyloid status.

Instead, preferential loss of cells or cellular components that rely more upon glycolysis, including synapses, axons, or glia, might explain why glycolysis decreases first in early AD. Loss of allostatic mechanisms and synaptic plasticity is another possible hypothesis.

In contrast to the loss of glycolysis in early dementia, asymptomatic individuals with amyloid positivity demonstrate preservation of the youthful pattern of brain AG when compared to cognitively normal individuals without amyloid pathology; a similar finding was not seen for the other metabolic parameters nor CBF. We suggest a few possible, and not mutually-exclusive, explanations for this intriguing finding. It is possible that increased AG in these individuals reflects resilience mechanisms that allow them to preserve their cognitive function despite amyloid pathology. Our results parallel a prior study showing that ^{18}FDG uptake was increased in select regions of highly cognitively resilient, aged individuals, including medial frontal and anterior cingulate areas, which typically show high AG during youth (34). Accordingly, much like Wald's famous analysis of survivorship bias when investigating bullet holes in returning wartime airplanes (35), the apparent "effects" of amyloid on brain metabolism in cognitively intact individuals might actually reflect resilience mechanisms to pathology, rather than amyloid-related damage. Cohort studies like these that require participant dedication, resources, and/or altruism might further potentiate selection bias toward individuals with such resilience to neurodegeneration. These collective effects, what we have previously described as "resilience bias" (36), might explain the relative preservation of brain AG in asymptomatic amyloid positive individuals seen here.

In vitro and animal studies have similarly shown that glycolysis is enhanced in amyloid-beta resistant neurons (37–40). There are several potential mechanisms by which increased neuronal glycolysis might support resilience to amyloid pathology. In addition to producing reduced nicotinamide adenine dinucleotide (NADH) for oxidative capacity, glycolysis supplies several other critical metabolic pathways, including lactate production, biosynthesis of lipids, nucleic and amino acids, and reducing oxidative stress, namely via the pentose phosphate pathway. Through these metabolic pathways, glycolysis might support homeostatic maintenance of neuronal networks and synaptic plasticity, which could compensate for early subclinical sites of damage and oxidative stress. The concept that youthful patterns of brain AG might reflect greater metabolic resilience to amyloid pathology might also help to explain why, at equivalent burdens of brain amyloid pathology, both chronological and brain age have been associated with an increased risk of cognitive impairment (41–43). Furthermore, disease progression and cognitive impairment might occur when pathology overcomes the protective mechanisms potentially related to AG.

It is also possible that the increased AG in preclinical AD represents a state of metabolic stress, which is then associated with amyloid deposition. Indeed, in young adults prior results have shown that brain amyloid preferentially deposits at sites of higher AG (22, 23). Moreover, there is increasing evidence that microglial activity, which relies upon increased AG, substantially influences the brain's response to amyloid pathology (44, 45). Thus, the relationship between AG and early amyloid pathology might be bidirectional. Increased metabolic demand and stress might lead to failure of proteostasis, thereby leading to amyloid deposition. Conversely, amyloid deposition might incite increased metabolic stress and demand, in part as a compensatory mechanism (46). Accordingly, a feed-forward loop might be established that could theoretically account for the accelerated "phase-transition" like change in amyloid deposition in the brain that is evident on longitudinal amyloid PET imaging (23). Several studies have shown that metabolic stressors increase amyloid aggregation in the brain and even in other tissues such as pancreatic islet cells (47–49) and transgenic *Caenorhabditis elegans* (50). Animal models will be helpful to elucidate the cellular and sub-cellular locations of changes in glycolysis in the context of AD pathology. Maintaining the supportive features of glycolysis while reducing metabolic demand might represent a means to forestall the progression of amyloid deposition worthy of further investigation.

Recently, we reported that cerebral small vessel disease, in which WMH burden is one of the defining characteristics, is associated with a relative increase in adjacent white matter glycolysis despite an overall loss of metabolism in WMH themselves (25). This finding parallels the increased gray matter glycolysis seen in the current study at sites of preclinical amyloid deposition, which subsequently decreases at the onset of symptomatic disease. One possible parsimonious explanation for both findings is that glycolysis might initially increase in response to local disease until that tissue is more significantly damaged. In the current study, we now also demonstrate that WMH burden is associated with loss of the youthful pattern of brain AG. This is consistent with our prior findings of relatively decreased total gray matter glycolysis in participants with cerebral small vessel disease (25). It is conceivable that WMH impact gray matter AG by disrupting the connectivity among different regions, thereby impairing both their function and ability to maintain allostasis. Hence, WMH might be a key factor in the loss of brain resilience to pathology, including in AD where it is increasingly recognized that WMH contribute to more rapid development of dementia (51–53). Intriguingly, in mice loss of white matter integrity might also be directly related to amyloid deposition and could impair the role of microglia in response to amyloid pathology (54). Further investigations are needed to more fully understand the association between WMH, AD, and brain metabolism (25, 55).

Our study has important strengths including being the largest multi-tracer metabolic PET imaging study of its kind. However, a few important limitations warrant discussion. To limit participant burden, the PET methods employed in this cohort did not include arterial lines to fully quantify measures of brain metabolism, and normalization methods were used to minimize batch effects and improve signal-to-noise, thereby limiting the inferences that can be made from these results. Future studies using quantitative PET methods are underway, including with higher intrinsic spatial resolution and signal-to-noise to obviate the need for normalization. In a portion of this cohort, contemporaneous amyloid assessment was not available; assuming amyloid negativity in these cases might have decreased the observed associations between amyloid positivity and brain metabolism by slightly diluting the amyloid negative sample. Another caveat in this study is that only a small number of individuals underwent longitudinal assessments; thus, our results could conceivably be confounded by generational cohort effects. Ongoing longitudinal studies of brain metabolism—ideally spanning decades—would be necessary to overcome this limitation.

In conclusion, our study suggests that a preserved/heightened youthful pattern of brain AG is associated with initial asymptomatic brain amyloid pathology, whereas loss of this pattern occurs alongside cognitive impairment in AD. WMH are shown to be one factor that reduces gray matter AG. Further research investigating mechanisms by which AG is preserved or lost in the aging brain might reveal new opportunities to improve brain resilience to pathology.

Methods

Participants and Regulatory Approvals. This study was performed according to the principles outlined within the Declaration of Helsinki. All participants and/or their designated healthcare power of attorney consented to participation in one

or more of these studies and for ongoing data analysis, as approved and overseen by the Washington University School of Medicine Institutional Review Board and the Radioactive Drug Research Committee. Data were gathered from participants enrolled in several different studies performed by the Vlassenko/Goyal (VG) Lab in the Neuroimaging Labs Research Center and the Knight Alzheimer Disease Research Center (ADRC), both at the Washington University School of Medicine in St. Louis.

A total of 285 individuals (55% women, self-reported sex/gender) aged 25 to 92 y were recruited from the Washington University community and the Knight ADRC. All participants had no neurological, psychiatric, or systemic medical illness that might compromise study participation. Individuals were excluded if they had contraindications to MRI, history of mental illness undergoing treatment, possible pregnancy, or medication use that could reliably interfere with brain function. Clinical cognitive status was assessed on the basis of the CDR (56) sum-of-boxes score (> 0 versus 0), or when CDR was unavailable, based on a combination of medical history, self-report, and other available global cognitive tests, preferentially the AD8 or Short Blessed Test, or as a last resort, the Montreal Cognitive Assessment corrected for education.

Brain Metabolism PET Imaging. All participants underwent metabolic brain PET and MRI structural imaging for registration and brain structure segmentation as previously described (17). All PET images were acquired in the eyes-closed waking state. No specific instructions were given regarding cognitive activity during scanning other than to remain awake. Briefly, ^{18}F-FDG, ^{15}O-O_2, ^{15}O-HO_2, and ^{15}O-CO PET scans were performed on participants in the awake, eyes-closed state, and processed to yield regional maps of CBF, $CMRO_2$, total CMRGlc, and AG (GI). Venous samples for plasma glucose determination were obtained just before and at the midpoint of the scan to verify that glucose levels were within normal range throughout the study, as well as to obtain blood radioactivity counts during the scan for future quantitative modeling. The PET images were blurred and resampled into the Desikan–Killiany atlas space (57). These registrations and their corresponding transformations were performed with in-house software. Individual head movement during scanning was restricted by a thermoplastic mask. GI was defined by the residuals after spatially regressing $CMRO_2$ from CMRGlc across all brain voxels, which correlates with regions where CMRGlc relatively exceeds that expected from $CMRO_2$ (26). Given the absence of absolute quantified measures of $CMRO_2$ and CMRGlc at the individual level due to the lack of arterial input functions and uncertainties surrounding the lumped constant, quantitative measures of AG (i.e., presuming a 6:1 stoichiometric relationship between oxygen and glucose use in the absence of AG) were not calculated in this study.

Each individual's GI, CMRGlc, CBF, and $CMRO_2$ images were partial volume corrected to regions defined by the Desikan–Killiany atlas and FreeSurfer subcortical parcellations. SUVR values were subsequently calculated for each segmented cortical and deep gray matter regions and scaled to have whole brain means of 1. Our routine partial volume corrected PET pipeline excludes results from the frontal and temporal poles, accumbens area, and parahippocampal region as these regions are highly vulnerable to noise artifact due to their location and size. All remaining regional data were than subjected to quantile normalization across PET sessions for each metabolic parameter, to account for known and unknown "batch effects" that might have occurred since the beginning of data collection in 2013. Though this normalization procedure removes quantitative information, it effectively retains rank topography while minimizing biases arising from such batch effects over time, including those related to scanner or radioactive tracer variability (17, 58).

Amyloid Brain PET Imaging. Research amyloid brain PET imaging was performed either with [11C]-labeled Pittsburgh Compound B (11C-PIB) (~ 12 mCi) or Florbetapir-F18 (~ 10 mCi), injected intravenously as a single bolus followed by 60 (^{11}C-PIB) or 70 (Florbetapir-F18) minutes of brain PET imaging. PET imaging was performed on a Siemens Biograph PET/CT or HR+ scanner (Siemens/CTI).

All available amyloid imaging underwent an in-house routine amyloid brain PET processing pipeline that included the following processing steps: framewise motion correction, registration to individual MRI T1 sequences, activity extraction within FreeSurfer v5.3 segmentations based on the Desikan-Killiany Atlas (57), and partial volume correction using the regional spread function implemented within a geometric transfer matrix framework, as has been described in detail previously (59–61). SUVR values were subsequently calculated for each segmented cortical and deep gray matter regions, referenced to the cerebellar gray matter (i.e., cerebellum SUVR = 1). A mean cortical SUVR (MC-SUVR) was calculated by averaging the SUVR values from prefrontal, parietal, and temporal cortical regions. Unless otherwise noted, a threshold MC-SUVR ≥ 1.42 is used to define a quantitatively "positive" amyloid ^{11}C-PIB scan, based on previously published studies (24, 62–64).

Amyloid status was considered to remain positive after any positive PET scan. Conversely, amyloid status was considered to have been negative for the duration prior to any negative amyloid test. Otherwise, amyloid status was determined based on amyloid testing performed within 2 y (or in one case, within 2.5 y) of the metabolic PET imaging. When a research amyloid scan was unavailable, the results from a clinical amyloid scan and/or CSF testing, if available, were used instead to determine amyloid status at the time of the metabolic PET session. When amyloid status was unavailable, it was assumed to be negative for statistical analyses unless proven otherwise.

MRI Imaging. MRI scans were obtained in all individuals to guide anatomic localization and identify specific gray matter regions. High-resolution structural images were acquired using 1.5T (Vision, Siemens) and 3T (Trio or Prisma, Siemens) scanners including a 3D sagittal T1-weighted magnetization-prepared 180° radio-frequency pulses and rapid gradient-echo (MPRAGE) sequence, with resolutions ranging from 0.8 × 0.8 × 0.8 mm to 1 × 1 × 1.3 mm. In a subset of individuals undergoing 3T MRI, 1 × 1 × 1 mm isotropic FLAIR sequences were obtained for WMH assessment.

FreeSurfer Analysis: FreeSurfer v5.3 software (57, 65, 66) was used to segment the brain into well-defined cortical and subcortical, gray and white matter regions of interest (ROIs) based on individual magnetization prepared rapid gradient echo (MPRAGE) MRI scans using the Desikan–Killiany and base FreeSurfer subcortical atlases. These ROIs were then used for the regional estimation of all PET metabolism parameters.

WMH Measurement. WMH severity was quantified by segmenting high signal intensity regions on individual FLAIR scans using the manually segmented intensity thresholds method. Each FLAIR scan was first preprocessed with tools in FMRIB Software Library (FSL) for brain extraction (67), bias field correction (68), and rigid body registration (69) to an individual's corresponding T1 image. For segmentation, an intensity threshold of ≥1.2 SD was applied with an in-house MATLAB script at each axial slice. This threshold has shown to maximize the sensitivity for manually identifying WMH, as applied in other neurodegenerative cohorts (70, 71). Manual tracings were then performed where needed by identifying true lesions from false positives due to motion, fat signal, ventricles, or other sources that would not be considered WMH. To ensure that all WMH clusters were fully represented, the manually selected clusters were treated as seed regions and allowed to expand one voxel outward all directions with a signal intensity restriction of ≥0.5 SD. All WMH binary masks were drawn by the same two raters. A neuroradiologist subsequently reviewed the WMH segmentations for accuracy.

Data, Materials, and Software Availability. The R script used to produce the figures and results is available upon request, edited to remove identifiers. Data availability is based on prior subject consents and the 2018 Common Rule (72). Coded, processed regional data prior to further data and statistical analyses are available from the study authors upon reasonable request by a qualified researcher following a data use agreement. Further requests for raw imaging data should be directed to the VG Lab and the Knight ADRC studies from which these data were gathered.

ACKNOWLEDGMENTS. We greatly appreciate Jennifer Byers and Kim Casey for their ongoing efforts in participant recruitment and acquiring data. We thank Abraham Z. Snyder, Matthew R. Brier, and Lars E. Couture for their advice on the analyses of the PET and MRI imaging data. We also thank other past and present members and students of the Vlassenko-Goyal lab for their assistance in data collection, management, and analysis. We are particularly grateful for our research participants and their families for their altruism. We also acknowledge the directors and staff of the Neuroimaging Labs Research Center, Knight Alzheimer's Disease Research Center, Center for Clinical Imaging Research (CCIR), and the Washington University cyclotron facility for making this research possible. Finally, we thank our reviewers for their critical and thoughtful questions and comments. Funding for this research was provided by the Barnes-Jewish Hospital Foundation (J.C.M.), the James S. McDonnell

Foundation, the McDonnell Center for Systems Neuroscience, the NIH/NIA R01AG053503 (A.G.V., M.E.R.), R01AG057536 (A.G.V., M.S.G.), RF1AG073210 (A.G.V., M.S.G.), P50AG0005681 (J.C.M.), P01AG026276 (J.C.M.), and P01AG003991 (J.C.M., T.L.-S.B.). Some of the MRI sequences used in the CCIR to produce the AMBR dataset were obtained from the Massachusetts General Hospital. Support for Florbetapir-F18 scans at the Knight ADRC was provided by Avid Radiopharmaceuticals, a wholly owned subsidiary of Eli Lilly.

Author affiliations: [a]Mallinckrodt Institute of Radiology, Washington University School of Medicine, St. Louis, MO 63110; [b]Department of Neurology, Washington University School of Medicine, St. Louis, MO 63110; [c]Neuroimaging Labs Research Center, Washington University School of Medicine, St. Louis, MO 63110; [d]Knight Alzheimer Disease Research Center, Washington University School of Medicine, St. Louis, MO 63108; [e]Department of Neuroscience, Washington University School of Medicine, St. Louis, MO 63110; [f]Program in Occupational Therapy, Washington University School of Medicine, St. Louis, MO 63108; [g]Department of Biomedical Engineering, Washington University School of Medicine, St. Louis, MO 63130; and [h]Department of Psychology & Brain Science, Washington University School of Medicine, St. Louis, MO 63130

1. T. Blazey, A. Z. Snyder, M. S. Goyal, A. G. Vlassenko, M. E. Raichle, A systematic meta-analysis of oxygen-to-glucose and oxygen-to-carbohydrate ratios in the resting human brain. *PLoS One* **13**, e0204242 (2018).
2. M. Segarra-Mondejar *et al.*, Synaptic activity-induced glycolysis facilitates membrane lipid provision and neurite outgrowth. *EMBO J.* **37**, e97368 (2018).
3. K. Chen *et al.*, Lactate transport facilitates neurite outgrowth. *Biosci. Rep.* **38**, BSR20180157 (2018).
4. U. Funfschilling *et al.*, Glycolytic oligodendrocytes maintain myelin and long-term axonal integrity. *Nature* **485**, 517–521 (2012).
5. J. Steiner *et al.*, Clozapine promotes glycolysis and myelin lipid synthesis in cultured oligodendrocytes. *Front. Cell Neurosci.* **8**, 384 (2014).
6. S. Ghosh, E. Castillo, E. S. Frias, R. A. Swanson, Bioenergetic regulation of microglia. *Glia* **66**, 1200–1212 (2018).
7. K. A. Nave, Myelination and the trophic support of long axons. *Nat. Rev. Neurosci.* **11**, 275–283 (2010).
8. R. A. Harris *et al.*, Aerobic glycolysis is required for spatial memory acquisition but not memory retrieval in mice. *eNeuro* **6** 1–9 (2019).
9. B. J. Shannon *et al.*, Brain aerobic glycolysis and motor adaptation learning. *Proc. Natl. Acad. Sci. U.S.A.* **113**, E3782–E3791 (2016).
10. D. A. Butterfield, B. Halliwell, Oxidative stress, dysfunctional glucose metabolism and Alzheimer disease. *Nat. Rev. Neurosci.* **20**, 148–160 (2019).
11. A. M. Brown, B. R. Ransom, Astrocyte glycogen as an emergency fuel under conditions of glucose deprivation or intense neural activity. *Metab. Brain Dis.* **30**, 233–239 (2015).
12. S. H. Baik *et al.*, A breakdown in metabolic reprogramming causes microglia dysfunction in Alzheimer's disease. *Cell Metab.* **30**, 493–507.e496 (2019).
13. R. Holland *et al.*, Inflammatory microglia are glycolytic and iron retentive and typify the microglia in APP/PS1 mice. *Brain Behav. Immun.* **68**, 183–196 (2018).
14. M. S. Goyal, M. Hawrylycz, J. A. Miller, A. Z. Snyder, M. E. Raichle, Aerobic glycolysis in the human brain is associated with development and neotenous gene expression. *Cell Metab.* **19**, 49–57 (2014).
15. D. K. Dastur, Cerebral blood flow and metabolism in normal human aging, pathological aging, and senile dementia. *J. Cereb. Blood Flow Metab.* **5**, 1–9 (1985).
16. U. Gottstein, K. Held, Effects of aging on cerebral circulation and metabolism in man. *Acta Neurol. Scand.* **60**, 54–55 (1979).
17. M. S. Goyal *et al.*, Loss of brain aerobic glycolysis in normal human aging. *Cell Metab.* **26**, 353–360. e353 (2017).
18. M. S. Goyal *et al.*, Persistent metabolic youth in the aging female brain. *Proc. Natl. Acad. Sci. U.S.A.* **116**, 3251–3255 (2019).
19. S. Hoyer, Abnormalities of glucose metabolism in Alzheimer's disease. *Ann. N. Y. Acad. Sci.* **640**, 53–58 (1991).
20. S. Hoyer, Brain glucose and energy metabolism abnormalities in sporadic Alzheimer disease. Causes and consequences: An update. *Exp. Gerontol.* **35**, 1363–1372 (2000).
21. M. Ogawa, H. Fukuyama, Y. Ouchi, H. Yamauchi, J. Kimura, Altered energy metabolism in Alzheimer's disease. *J. Neurol. Sci.* **139**, 78–82 (1996).
22. A. G. Vlassenko *et al.*, Spatial correlation between brain aerobic glycolysis and amyloid-beta (Abeta) deposition. *Proc. Natl. Acad. Sci. U.S.A.* **107**, 17763–17767 (2010).
23. M. S. Goyal *et al.*, Spatiotemporal relationship between subthreshold amyloid accumulation and aerobic glycolysis in the human brain. *Neurobiol. Aging* **96**, 165–175 (2020), 10.1016/j.neurobiolaging.2020.08.019.
24. A. G. Vlassenko *et al.*, Aerobic glycolysis and tau deposition in preclinical Alzheimer's disease. *Neurobiol. Aging* **67**, 95–98 (2018).
25. M. R. Brier *et al.*, Increased white matter glycolysis in humans with cerebral small vessel disease. *Nat. Aging* **2**, 991–999 (2022).
26. S. N. Vaishnavi *et al.*, Regional aerobic glycolysis in the human brain. *Proc. Natl. Acad. Sci. U.S.A.* **107**, 17757–17762 (2010).
27. I. Beheshti, S. Nugent, O. Potvin, S. Duchesne, Disappearing metabolic youthfulness in the cognitively impaired female brain. *Neurobiol. Aging* **101**, 224–229 (2021).
28. J. Lee *et al.*, Deep learning-based brain age prediction in normal aging and dementia. *Nat. Aging* **2**, 412–424 (2022).
29. A. Z. Wagen *et al.*, Life course, genetic, and neuropathological associations with brain age in the 1946 British Birth Cohort: A population-based study. *Lancet Healthy Longev* **3**, e607–e616 (2022).
30. I. K. Yeo, R. A. Johnson, A new family of power transformations to improve normality or symmetry. *Biometrika* **87**, 954–959 (2000).
31. C. K. Morse, Does variability increase with age? An archival study of cognitive measures. *Psychol. Aging* **8**, 156–164 (1993).
32. Q. Tian *et al.*, The brain map of gait variability in aging, cognitive impairment and dementia-A systematic review. *Neurosci. Biobehav. Rev.* **74**, 149–162 (2017).
33. P. M. Thompson *et al.*, Cortical variability and asymmetry in normal aging and Alzheimer's disease. *Cereb. Cortex.* **8**, 492–509 (1998).
34. E. M. Arenaza-Urquijo *et al.*, The metabolic brain signature of cognitive resilience in the 80+: Beyond Alzheimer pathologies. *Brain* **142**, 1134–1147 (2019).
35. A. Wald, *A Reprint of'A Method of Estimating Plane Vulnerability Based on Damage of Survivors* (Center for naval analyses alexandria va operations evaluation group, 1980).
36. M. S. Goyal, A. G. Vlassenko, M. E. Raichle, Reply to Biskup et al. and Tu et al.: Sex differences in metabolic brain aging. *Proc. Natl. Acad. Sci. U.S.A.* **116**, 10634–10635 (2019).
37. T. Soucek, R. Cumming, R. Dargusch, P. Maher, D. Schubert, The regulation of glucose metabolism by HIF-1 mediates a neuroprotective response to amyloid beta peptide. *Neuron* **39**, 43–56 (2003).
38. J. T. Newington *et al.*, Amyloid beta resistance in nerve cell lines is mediated by the Warburg effect. *PLoS One* **6**, e19191 (2011).
39. A. Lone, R. A. Harris, O. Singh, D. H. Betts, R. C. Cumming, p66Shc activation promotes increased oxidative phosphorylation and renders CNS cells more vulnerable to amyloid beta toxicity. *Sci. Rep.* **8**, 17081 (2018).
40. C. Arias, T. Montiel, R. Quiroz-Baez, L. Massieu, beta-Amyloid neurotoxicity is exacerbated during glycolysis inhibition and mitochondrial impairment in the rat hippocampus in vivo and in isolated nerve terminals: Implications for Alzheimer's disease. *Exp. Neurol.* **176**, 163–174 (2002).
41. S. E. Schindler *et al.*, Predicting symptom onset in Sporadic Alzheimer disease with amyloid pet. *Neurology* **97**, e1823–e1834 (2021).
42. P. R. Millar *et al.*, Predicting brain age from functional connectivity in symptomatic and preclinical Alzheimer disease. *Neuroimage* **256**, 119228 (2022), 10.1016/j.neuroimage.2022.119228.
43. J. H. Cole, R. E. Marioni, S. E. Harris, I. J. Deary, Brain age and other bodily "ages": Implications for neuropsychiatry. *Mol. Psychiatry* **24**, 266–281 (2019).
44. F. Leng, P. Edison, Neuroinflammation and microglial activation in Alzheimer disease: Where do we go from here? *Nat. Rev. Neurol.* **17**, 157–172 (2021).
45. D. S. Knopman *et al.*, Alzheimer disease. *Nat. Rev. Dis. Primers* **7**, 33 (2021).
46. R. Santangelo *et al.*, Beta-amyloid monomers drive up neuronal aerobic glycolysis in response to energy stressors. *Aging* **13**, 18033–18050 (2021).
47. J. Montane, A. Klimek-Abercrombie, K. J. Potter, C. Westwell-Roper, C. Bruce Verchere, Metabolic stress, IAPP and islet amyloid. *Diabetes Obes. Metab.* **14**, 68–77 (2012).
48. L. Gasparini *et al.*, Effect of energy shortage and oxidative stress on amyloid precursor protein metabolism in COS cells. *Neurosci. Lett.* **231**, 113–117 (1997).
49. Z. Cai, B. Zhao, A. Ratka, Oxidative stress and beta-amyloid protein in Alzheimer's disease. *Neuromol. Med.* **13**, 223–250 (2011).
50. E. Teo *et al.*, Metabolic stress is a primary pathogenic event in transgenic Caenorhabditis elegans expressing pan-neuronal human amyloid beta. *Elife* **8**, e50069 (2019).
51. F. A. Provenzano *et al.*, White matter hyperintensities and cerebral amyloidosis: Necessary and sufficient for clinical expression of Alzheimer disease? *JAMA Neurol.* **70**, 455–461 (2013).
52. M. Radanovic *et al.*, White matter abnormalities associated with Alzheimer's disease and mild cognitive impairment: A critical review of MRI studies. *Expert Rev. Neurother.* **13**, 483–493 (2013).
53. Y. L. Wang *et al.*, Associations of white matter hyperintensities with cognitive decline: A longitudinal study. *J. Alzheimers Dis.* **73**, 759–768 (2020).
54. C. Depp *et al.*, Ageing-associated myelin dysfunction drives amyloid deposition in mouse models of Alzheimer's disease. bioRxiv 2021.07.31.454562 (2021), https://doi.org/10.1101/2021.1107.1131.454562 Accessed 28 October 2022.
55. A. T. Restrepo *et al.*, Axo-vascular coupling mediated by oligodendrocytes. bioRxiv 2022.06.16.495900 (2022), https://doi.org/10.1101/2022.1106.1116.495900 Accessed 28 October 2022.
56. J. C. Morris, The Clinical Dementia Rating (CDR): Current version and scoring rules. *Neurology* **43**, 2412–2414 (1993).
57. R. S. Desikan *et al.*, An automated labeling system for subdividing the human cerebral cortex on MRI scans into gyral based regions of interest. *Neuroimage* **31**, 968–980 (2006).
58. J. T. Leek *et al.*, Tackling the widespread and critical impact of batch effects in high-throughput data. *Nat. Rev. Genet.* **11**, 733–739 (2010).
59. Y. Su *et al.*, Partial volume correction in quantitative amyloid imaging. *Neuroimage* **107**, 55–64 (2015).
60. Y. Su *et al.*, Utilizing the Centiloid scale in cross-sectional and longitudinal PiB PET studies. *Neuroimage Clin.* **19**, 406–416 (2018).
61. Y. Su *et al.*, Comparison of Pittsburgh compound B and florbetapir in cross-sectional and longitudinal studies. *Alzheimers Dement (Amst)* **11**, 180–190 (2019).
62. C. R. Jack Jr., *et al.*, Age-specific and sex-specific prevalence of cerebral beta-amyloidosis, tauopathy, and neurodegeneration in cognitively unimpaired individuals aged 50–95 years: A cross-sectional study. *Lancet Neurol.* **16**, 435–444 (2017).
63. M. A. Mintun *et al.*, [11C]PIB in a nondemented population: Potential antecedent marker of Alzheimer disease. *Neurology* **67**, 446–452 (2006).
64. Y. Su *et al.*, Quantitative analysis of PiB-PET with FreeSurfer ROIs. *PLoS One* **8**, e73377 (2013).
65. B. Fischl *et al.*, Whole brain segmentation: Automated labeling of neuroanatomical structures in the human brain. *Neuron* **33**, 341–355 (2002).
66. B. Fischl *et al.*, Automatically parcellating the human cerebral cortex. *Cereb. Cortex.* **14**, 11–22 (2004).
67. S. M. Smith, Fast robust automated brain extraction. *Hum. Brain Mapp.* **17**, 143–155 (2002).
68. Y. Zhang, M. Brady, S. Smith, Segmentation of brain MR images through a hidden Markov random field model and the expectation-maximization algorithm. *IEEE Trans. Med. Imaging* **20**, 45–57 (2001).
69. M. Jenkinson, S. Smith, A global optimisation method for robust affine registration of brain images. *Med. Image Anal.* **5**, 143–156 (2001).
70. N. A. Hubbard *et al.*, Calibrated imaging reveals altered grey matter metabolism related to white matter microstructure and symptom severity in multiple sclerosis. *Hum. Brain Mapp.* **38**, 5375–5390 (2017).
71. J. Strain *et al.*, Depressive symptoms and white matter dysfunction in retired NFL players with concussion history. *Neurology* **81**, 25–32 (2013).
72. J. Menikoff, J. Kaneshiro, I. Pritchard, The common rule, updated. *N. Engl. J. Med.* **376**, 613–615 (2017).